RESEARCH ARTICLE

Check for updates

Organic/inorganic hydrogels by simultaneous self-assembly and mineralization of aromatic short-peptides†

Mari C. Mañas-Torres, [a] Gloria B. Ramírez-Rodríguez, *[b] José I. García-Peiro,[c] Belén Parra-Torrejón, [b] Juan M. Cuerva, [a] Modesto T. Lopez-Lopez, [d,e] Luis Álvarez de Cienfuegos *[a,e] and José M. Delgado-López [b]

Self-assembled peptides and proteins have turned out to be excellent templates for the growth of inorganic minerals and can be used to emulate natural biomineralization processes. Doing this, researchers have developed complex sophisticated materials with properties, in some cases, similar to those found in nature. Of special interest is the development of scaffolds able to guide bone regeneration. The bone tissue comprises an organic matrix composed of aligned collagen fibers containing nanoapatite crystals oriented along the fiber direction. During bone mineralization, both processes, the self-assembly of collagen fibrils and mineralization occur simultaneously. Collagen fibers are able to control calcium phosphate nucleation and subsequent apatite crystal growth at a very limited range of collagen density and ionic concentration. In this study, we reproduced the simultaneity of both processes using an artificial peptide fluorenylmethoxycarbonyl-diphenylalanine (Fmoc-FF) that has the ability to self-assemble in water after the addition of Ca^{2+} ions. Therefore, the peptide self-assembly process and the mineralization of apatite are Ca-demanding processes and occur simultaneously. The role of peptide and ionic concentrations has been investigated affording organic/inorganic hybrid hydrogels with different degrees of homogeneity and mineralization. Interestingly, at very low Ca^{2+} concentrations, we found that apatite nanocrystals are integrated into Fmoc-FF fibrils and oriented as in biologically mineralized collagen fibrils, the basic building blocks of bone.

Introduction

Amphiphilic short-peptides are able to self-assemble in water giving rise to supramolecular polymers.[1–4] At specific concentrations, these peptides are able to form extended intertwining networks of fibers that immobilize the liquid solution, giving rise to hydrogels. Significant examples are Fmoc-dipeptide derivatives.[5–7] These gels have found interesting technological applications in fields, such as tissue engineering,[8–10] drug

delivery,[11–13] protein crystallization, *etc.*[14–17] These peptides are able to self-assemble under different stimuli, such as temperature, solvent or pH switch, addition of salts, or enzymatic reactions.[7,18,19] It has been shown that these stimuli can have an effect on the mechanism of self-assembly and on the physical properties of the resulting gels.[20–23] Moreover, the non-covalent interactions between monomers can also be altered or inhibited by the presence of different additives in the reaction media.[24–26] As such, the desired properties of the resulting hydrogels can be substantially different if the additives are introduced before or after gelation. This factor is crucial if hybrid or composite hydrogels are intended.[27,28] In fact, it has been proven that the incorporation of different polymers,[29,30] metallic nanoparticles[31,32] and carbon materials[15,33–35] modifies the mechanical properties of the resulting gels. Before gelation the impact of the additives on the gel properties can be due to the capacity of these substances to alter the peptide self-assembly process. On the other hand, the promotion of self-assembly in the presence of additives can maximize the interactions between both materials giving rise to more homogeneous hybrid and/or composite materials.

[a]Dpto de Química Orgánica, Facultad de Ciencias, Unidad de Excelencia Química Aplicada a Biomedicina y Medioambiente, Universidad de Granada (UGR), 18071-Granada, Spain. E-mail: lac@ugr.es
[b]Dpto de Química Inorgánica, Facultad de Ciencias, Unidad de Excelencia Química Aplicada a Biomedicina y Medioambiente (UGR), Spain. E-mail: gloria@ugr.es
[c]Instituto de Nanociencia y Materiales de Aragón, CSIC-Universidad de Zaragoza, 50009, Zaragoza, y Departamento de Ingeniería Química y Tecnología Medioambiental (IQTMA), Universidad de Zaragoza, 50018 Zaragoza, Spain
[d]Dpto de Física Aplicada, Facultad de Ciencias, (UGR), Spain
[e]Instituto de Investigación Biosanitaria ibs.GRANADA, Spain
†Electronic supplementary information (ESI) available: Experimental part and supplementary figures. See DOI: 10.1039/d1qi01249e

This journal is © the Partner Organisations 2022

Inorg. Chem. Front., 2022, **9**, 743–752 | 743

On top of that, additional factors have to be taken into account if additives are expected to grow or assemble *in situ*, that is, in the hydrogel media, mimicking the conditions occurring in a biomineralization process (*e.g.*, bone mineralization).[36] In this scenario, composite gels are formed *in situ* from simpler building units of the components, the peptide fibers and the additives, by two processes occurring simultaneously, the self-assembly and mineralization.[37] Herein, the time at which these two processes occur and the degree of interaction between both components during growth determine the formation and homogeneity of the resulting hybrid or composite gel.

Considering this, herein we obtained hybrid hydrogels by simultaneously combining the self-assembly of an aromatic short-peptide, Fmoc-FF (fluorenylmethoxycarbonyl-diphenylalanine) and the mineralization of nanocrystalline hydroxyapatite (HA, $Ca_{10}(PO_4)_6(OH)_2$), starting from its ionic precursors. Since the self-assembly of Fmoc-FF is triggered by Ca^{2+}, both processes (self-assembly and mineralization) are interconnected, maximizing the interactions and interplay between the organic/inorganic phases and favoring the formation of more homogeneous hybrid hydrogels. Furthermore, Fmoc-AA (Fmoc-dialanine), a known peptide able to form weak hydrogels[26,38,39] have also been used to further shed light on the influence of peptide's self-assembly in the biomineralization process.

Previous reports on mineralization of self-assembled supramolecular peptides studied the growth of the mineral from a preexisting supramolecular polymeric network,[40–44] similar to works carried out on polymeric hydrogels.[45,46] Stupp *et al.* demonstrated the potential of amphiphilic peptide fibers to control the crystallization of oriented apatite nanocrystals, showing that the morphologies of the nanofibers play a relevant role in templating apatite crystallization.[41,44] The mineralization of the Fmoc-FF hydrogel has been carried out and a hybrid hydrogel with increased thermal stability, stiffness, and resistance to breakage under tension has been obtained.[42] A similar result has been obtained by incorporating apatite nanoparticles into co-assembled Fmoc-FF and Fmoc-arginine hydrogels.[43]

On the other hand, bone mineralization has been largely investigated to understand its fascinating biomechanical properties and structure–function relationship and as a source of inspiration for the development of sophisticated materials with highly controllable and specialized functions.[47–50] During bone mineralization, collagen fibers serve as a structural template controlling both calcium phosphate nucleation and subsequent apatite crystal growth, playing a predominant role in determining the size and 3D distribution of the mineral.[51] This precise control occurs under a very limited range of collagen density and ionic concentration (calcium, phosphate and carbonate) with both processes, *i.e.* self-assembly of collagen fibrils and mineralization occurring simultaneously.[51] Herein, the fine tuning of the initial peptide and ionic concentration have allowed us to reproduce, in a more precise manner, biomineralization conditions showing, for the first

time, that substoichiometric Ca^{2+} concentrations give rise to nanoapatite crystals embedded and perfectly oriented along the peptide fibers.

Experimental

Reagents and materials

Calcium chloride dihydrate ($CaCl_2 \cdot 2H_2O$, ACS reagent, ≥99%), sodium phosphate dibasic (Na_2HPO_4, BioXtra, ≥99%), sodium citrate dihydrate ($Na_3(C_6H_5O_7) \cdot 2H_2O$, ≥99%) and sodium carbonate (Na_2CO_3, BioXtra, ≥99%) were purchased from Sigma Aldrich. All solutions were prepared with ultrapure water (0.22 μS, 25 °C, Milli-Q©, Millipore). *N*-Fluorenylmethoxycarbonyl-diphenylalanine (Fmoc-FF) and *N*-fluorenylmethoxycarbonyl-dialanine (Fmoc-AA) were purchased from Bachem Co., Switzerland, and were used without further purification.

Mineralization of aromatic short-peptides

All the experiments were carried out in a 10 mL vial. 1.27 g of peptide solution (20 mM, pH = 10.2, adjusted with NaOH) was weighted in a 10 mL vial. Then, 420 μL of Na_2HPO_4 solution (120 mM), 420 μL of Na_3Cit solution (100 mM) and 420 μL of Na_2CO_3 solution (100 mM) were added and mixed vigorously by vortexing. The pH of the solution was 10.4. Finally, 420 μL of $CaCl_2$ solution (200 mM) was added to trigger the simultaneous self-assembly and mineralization of peptide. The precipitation of calcium phosphate prompted a slight decrease of the pH (pH = 9). The final molar concentrations of the peptide and of the mineralizing solutions are summarized in Table 1. The Ca/P molar ratio was 1.67, corresponding to the stoichiometric value of hydroxyapatite. Then, the mixture was aged at 37 °C without disturbing, leading to the formation of hybrid hydrogels. After 24 hours, the mineralized hydrogels were repeatedly washed with ultrapure water by centrifugation (7500 rpm, 3 min) and freeze-dried overnight under vacuum (Telstar Cryodos freeze-drier). HA crystallization was also carried out in the absence of peptides as a control. Non-mineralized Fmoc-FF and Fmoc-AA gels were prepared through the same procedure without the addition of phosphate solution to avoid HA crystallization.

Fmoc-FF hydrogels were selected for further studies. Hybrid materials were prepared at increasing nominal mineral/organic weight ratios maintaining constant the concentration of mineralizing solutions and varying the peptide concentration, as indicated in Table 2. Hybrid Fmoc-FF hydrogels

Table 1 Final molar concentrations of reactants (mM) for each experiment. Fmoc-FF and Fmoc-AA are named FF and AA, respectively

Sample name	Peptide	Na_2HPO_4	Na_2CO_3	Na_3Cit	$CaCl_2$
AA-HA	4.7	10	8.33	8.33	16.67
FF-HA	4.7	10	8.33	8.33	16.67
HA	—	10	8.33	8.33	16.67
AA	4.7	—	8.33	8.33	16.67
FF	4.7	—	8.33	8.33	16.67

744 | *Inorg. Chem. Front.*, 2022, **9**, 743–752

This journal is © the Partner Organisations 2022

Table 2 Final molar concentrations of reactants (mM) for the preparation of hybrid Fmoc-FF hydrogels

Sample name	Fmoc-FF	Na_2HPO_4	Na_2CO_3	Na_3Cit	$CaCl_2$
80/20	0.8	10	8.33	8.33	16.67
60/40	2.1	10	8.33	8.33	16.67
40/60[a]	4.7	10	8.33	8.33	16.67
20/80	12.5	10	8.33	8.33	16.67
Ca1	4.7	10	8.33	8.33	2
Ca2	4.7	10	8.33	8.33	8.3
Ca3	4.7	10	8.33	8.33	11.11
Ca4[a]	4.7	10	8.33	8.33	16.67
Ca5	4.7	10	8.33	8.33	33.3

[a] 40/60 and Ca4 are the same experiments, corresponding to a Ca/P molar ratio of 1.67, stochiometric value of hydroxyapatite ($Ca_{10}(PO_4)_6(OH)_2$).

were also prepared in the presence of increasing calcium ion concentrations (Table 2).

Characterization of hybrid materials

Gel formation was visually evaluated by the inverted vial method.

Transmission electron microscopy (TEM) images were recorded with a LIBRA 120 PLUS instrument (Carl Zeiss SMT, Centre for Scientific Instrumentation of the University of Granada, CIC-UGR), operating at 120 kV. A small portion of the synthesized hydrogel was deposited on conventional copper grids and incubated for several minutes. Then, the grids were washed with ultrapure water six times (drops of 30 μL) and left to air-dry under ambient conditions. TEM samples were not stained (neither with osmium nor with uranyl acetate) since apatite nanocrystals and stain precipitates are sometimes indistinguishable from each other.

High-angle annular dark field-scanning transmission electron microscopy (HAADF-STEM) images, energy-dispersive X-ray (EDS) spectra and selected-area electron diffraction (SAED) patterns of different areas of FF-HA sample were acquired with a STEM FEI TALOS F200X microscope equipped with a 4 Super-X SDDs (Thermo Fisher Scientific Waltham, MA, USA) of CIC-UGR.

Cryo-scanning electron microscopy (Cryo-SEM) imaging was performed using an ESEM Quanta 650 FEG (ThermoFisher-FEI) microscope equipped with a cryo system (Quorum Technologies, model PP3010T). The hydrogel was sublimated at −90 °C for 7 min, then the sample were loaded on the cryo-specimen holder and cryo-fixed in slush nitrogen (−210 °C) and finally quickly transferred to the cryo-unit in the frozen state.

X-ray powder diffraction (XRPD) data were collected on a Bruker D8 Discover diffractometer by using Cu Kα radiation (λ = 1.5406 Å) and a PILATUS3R 100K-A detector. The data were collected from 5° to 50° (2θ) with a scan rate of 3 s per step, step size of 0.02° and a HV generator set at 50 kV and 1 mA.

Fourier transform infrared (FTIR) spectra of xerogels were recorded on a Tensor 27 (Bruker, Karlsruhe, Germany) spectrometer. 2 mg of the sample was mixed with 200 mg of anhydrous potassium bromide (KBr) and pressed at 5 tons into a 12 mm diameter disc using a hydraulic press (Specac). A pure KBr disk was used as a blank. The infrared spectra were recorded by accumulating 25 scans covering from 400 cm^{-1} to 4000 cm^{-1} at a resolution of 3 cm^{-1}.

Thermogravimetry analysis (TGA) of xerogels was carried out in a Mettler-Toledo TGA/DSC1 thermal balance (Mettler-Toledo International Inc., Switzerland, from CIC-UGR) with a heating rate of 10 °C min^{-1} up to 900 °C under a nitrogen flow.

Rheological characterization

The measurements were made using a Haake MARS III controlled-stress rheometer (Thermo Fisher Scientific, Waltham, MA, USA) at a constant temperature of 37 ± 0.1 °C. For each set of experimental conditions, we measured at least 3 different samples. The mean values and standard deviations of each magnitude are provided in this work.

Gelation kinetics studies. The studies were made using a double cone-plate geometry (60 mm in diameter and 2° angle; sensor DC60/2° Ti L, Thermo Fisher Scientific, Waltham, MA, USA). In measurements, the gap between the double cone and the plate of the rheometer was equal to the truncation of the cone (0.088 mm), and a sample volume of 6 mL was required for this sensor. The hydrogels were generated directly in this geometry prior to the measurement and we monitored the viscoelastic moduli (storage modulus, G', and loss modulus, G'') for 3 h, for an oscillatory strain of fixed amplitude (0.001) and frequency (1 Hz).

Rheological behaviour under oscillatory shear strain. After the 24 h gelation period was completed, the rheological properties of hydrogels were measured using a plate–plate geometry of 35 mm diameter (sensor P35 Ti L S serrated). First, we carried out ramps of oscillatory strains of increasing amplitude and constant frequency (1 Hz), from which we obtained the values of the storage (G') and loss (G'') moduli as a function of the amplitude of the oscillatory shear strain, γ_0. From these curves of G' and G'' as a function of γ_0 (amplitude sweeps) we delimited the extension of the linear viscoelastic region (LVR). Then we subjected the samples to ramps of fixed shear strain amplitude (γ_0 = 0.0002), well into the LVR, and increasing frequency in the range of 0.1–15 Hz (frequency sweeps).

Results and discussion

We first evaluated the relationship between the peptide composition and its ability to form hybrid mineralized hydrogels. Two aromatic short-peptides, i.e., Fmoc-FF and Fmoc-AA were studied. Their assembly and mineralization were carried out simultaneously via a protocol inspired by bone biomineralization.[52,53] The peptide solution was mixed by vortexing with a solution containing phosphate, carbonate and citrate, the two latter being important components of bone nanoapatite.[52,54–56] Then, a calcium-containing solution was added to the latter mixture triggering the simultaneous self-assembly and mineralization of peptide fibrils. After 24 hours, the sample containing Fmoc-FF (FF-HA) showed the formation

This journal is © the Partner Organisations 2022

*Inorg. Chem. Front.*, 2022, **9**, 743–752 | **745**

of a weak translucent hydrogel that was not able to self-support after vial inversion (inset Fig. 1a). A sample containing Fmoc-AA (AA-HA) showed the formation of individual white aggregates but not a hydrogel (inset Fig. 1b). The TEM image of FF-HA showed the presence of a dense mesh of long fibers formed by the self-assembly of Fmoc-FF in the presence of Ca^{2+}. Interestingly, most of these fibers were exhaustively decorated with nanocrystals of HA that appeared homogeneously distributed for all the visualized area, likewise peptide fibers (Fig. 1a). In contrast, TEM images of AA-HA showed the presence of higher amounts of HA nanocrystals arranged in dense aggregates, similar to the mineralization of HA in the practical absence of peptide fibers (Fig. S1a†). These results showed that under these conditions, a competition between peptides and the phosphate ions for the Ca^{2+} ion occurred. It is known that in water the hydrophobic effect is the major driving force for the self-assembly of aromatic short-peptides. Thus, more hydrophobic peptides have a major tendency to self-assemble into supramolecular polymers. It is also known that metal ions are able to promote the self-assembly of aromatic peptides having an impact on the early stages of self-assembly, influencing the kinetics of the process, the secondary structure of the resulting aggregates, and the mechanical and self-healing properties of the resulting hydrogels. Nevertheless, the magnitude of this effect depends also of the hydrophobicity of the peptide. We have recently proven that Fmoc-FF in the presence of Ca^{2+} has a higher tendency and faster kinetics to self-assembly into long fibers than Fmoc-AA, giving rise to more rigid hydrogels. Considering this, and based on the images obtained by TEM of both samples, we can infer that cross-linking of the supramolecular structure by calcium ions not only enhances the stability of hydrogels but also acts as reactive sites for calcium phosphate nucleation and growth. In contrast, in AA-HA, the absence of peptide fibers suggests that Ca^{2+} ions have been mainly used to promote the growth of HA. In fact, TEM images showed a higher density of HA nanocrystals that are closely interacting forming large aggregates (Fig. 1b). It is difficult to observe mineralized peptide fibers in these images. As commented above, the different behaviour in this sample might only be explained by the weaker and/or

slower capacity of Fmoc-AA to self-assemble. Control experiments in the absence of phosphate to avoid peptide mineralization revealed that Fmoc-AA peptides did not form a hydrogel and show globular morphology in TEM images (Fig. S1b†). While Fmoc-AA was not able to self-assembly into fibers, Fmoc-FF peptides formed hydrogels through self-assembly of peptide fibers similar to that previously found on hybrid FF-HA hydrogels (Fig. S1c†).

To analyse in more detail, the as-synthesized samples were washed with ultrapure water, freeze-dried and characterized by FTIR, XRD and TGA. XRD pattern of the control Fmoc-FF sample (Fig. S2a†) revealed that the presence of calcite, due to the fact that this sample was prepared through the same mineralization protocol but without adding phosphate, triggered the precipitation of calcium carbonate, a poorly soluble salt hard to eliminate through the washing procedure. The TGA curve of this sample (Fig. S2b†) presents three weight losses at around 200 °C, 324 °C and 710 °C. The two first weight losses belong to the degradation of the Fmoc-FF peptide which completely disappeared at 440 °C.[15] The weight loss at 710 °C is due to the decarbonation of calcite ($CaCO_3 \rightarrow CO_2 + CaO$),[57] retaining a residual mass at 900 °C of 17 wt%. On the other hand, XRD patterns of HA, FF-HA and AA-HA samples (Fig. S2a†) display two broad Bragg peaks at around 26° and 32° (2θ) ascribed to the poor crystallinity of apatite. Indeed, the FTIR spectra of HA, AA-HA and FF-HA (Fig. 2a) show typical phosphate vibrational bands of poorly crystalline apatite ($\nu_4 PO_4$ at 561 and 602 cm^{-1} and $\nu_3 PO_4$ at 1032, 1046 and 1087 cm^{-1}), those containing citrate ($\nu_{as}COO^-$ at 1599 cm^{-1}) and carbonate ($\nu_3 CO_3$ at 1431 and 1491 cm^{-1}).[56] This finding reveals that biomimetic mineralization of short aromatic peptides allows to obtain apatite nanoparticles mimicking the poor crystallinity and composition of bone apatite, taking into account that carbonate entails 4–6 wt% of bone apatite composition and citrate accounts for 5.5 wt% of the organic bone matter.[56] This subtle nuance is of paramount importance since the current challenges in bone tissue engineering are engineering biomaterials with a new level of functionality that attempts to mimic biochemical and biophysical cues from the bone extracellular matrix.[58] Hence, biomimetic mineralized synthetic peptides are proposed as potential candidates for bone regeneration due to their osteoconductive and
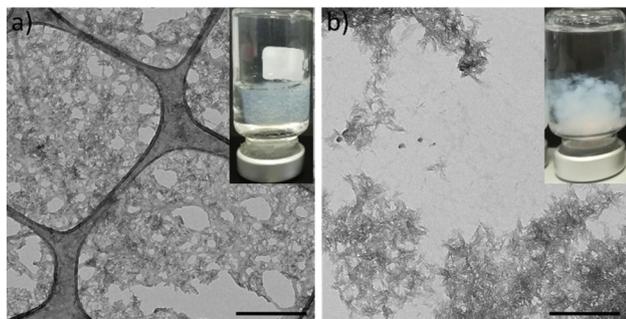
Fig. 1 TEM images of FF-HA (a) and AA-HA (b) unstained samples. Scale bar = 500 nm. Insets show images of inverted vials under each condition.
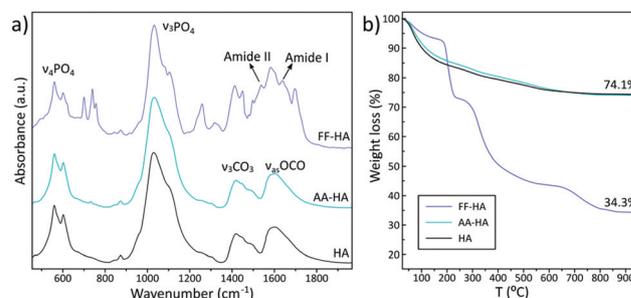

Fig. 2 FTIR spectra (a) and TGA curves (b) of freeze-dried FF-HA and AA-HA samples. Data of HA (control) are also shown for comparison.

746 | *Inorg. Chem. Front.*, 2022, **9**, 743–752

This journal is © the Partner Organisations 2022

osteoinductive properties.[59,60] The FTIR spectrum of FF-HA (Fig. 2a) additionally shows vibrational bands of Fmoc-FF such as the C=O stretching band (amide I) at 1651 cm^{-1} and the N–H bending band (amide II) at 1534 cm^{-1}.[32] The TGA curve of FF-HA (Fig. 2b) confirmed the formation of hybrid hydrogel containing 66 wt% peptide and 34 wt% mineral phase (*i.e.*, apatite). On the other hand, the FTIR spectrum of AA-HA (Fig. 2a) revealed the null presence of peptide AA, which was further confirmed by TGA. The thermal degradation of AA-HA (Fig. 2b) exhibited the same weight loss as the control sample (HA) confirming the absence of the peptide. These results, aside from revealing the weak intermolecular forces between Fmoc-AA molecules and thus the limited stability of the hydrogel in water, confirm the poor chemical interaction between the peptide and the mineral phase. On this basis, it is clear that FF-HA hydrogels maintained a stable hybrid supramolecular structure even after several cycles of washing. This effect could be associated with the dual role of calcium ions in the formation of the hybrid hydrogel: (i) acting as a crosslinking agent of peptide fibres and (ii) acting as sites for the nucleation and growth of calcium phosphate.

Considering this, we selected Fmoc-FF to study the properties of the resulting hybrid hydrogels. First, we studied the impact of the initial inorganic/organic (HA/FF) weight ratios during the mineralization process by increasing concentrations of Fmoc-FF: 0.8 mM, 2.1 mM, 4.7 mM and 12.5 mM (see Table 2). The 80/20 sample did not form a gel but rather white aggregates similar to the HA-AA sample (Fig. S3†). TEM image of this sample showed HA nanocrystals while peptide fibers were not observed (Fig. 3a). The 60/40 and 40/60 samples formed translucent homogeneous hydrogels, hydrogel 60/40 being apparently opaquer (Fig. S3†). In both cases, hydrogels showed clear syneresis due to the rigidification and contraction of the solid part of the hydrogel induced by the biomineralization process (Fig. S3†).

Peptide fibers extensively decorated with HA nanocrystals were observed in TEM images of both samples (Fig. 3b and c). As an important difference, the 60/40 sample exhibited local areas with a higher accumulation of HA nanocrystals, suggesting that mineralization also occurred in solution. In contrast, the reduction of the mineral fraction (40/60) resulted in the homogeneous mineralization of fibers. Indeed, the peptide fibers were more clearly identified and the HA nanocrystals (Ca and P signals were identified by XEDS, Fig. S4†) were integrated into the organic matrix, giving a more homogeneous hybrid hydrogel. A further analysis of this hydrogel by cryo-SEM (Fig. 3e and f) revealed rough surfaces due to the integration of the mineral phase into the organic matrix, as previously observed in the SEM images of the biomimetic mineralized peptide.[59,60] Furthermore, the presence of globular particles along the peptide fibers (zoom of Fig. 3f) seems to indicate a homogeneous distribution of the apatite nanocrystals in the organic matrix. Finally, the 20/80 sample formed a rigid hydrogel composed of a dense mesh of peptide fibers with scarce amounts of HA nanocrystals bound to the peptide network (Fig. 3d).
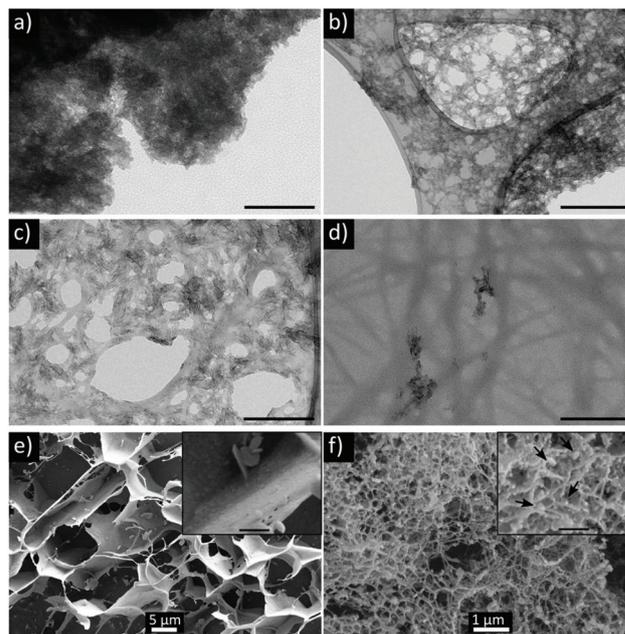
Fig. 3 TEM images of hybrid hydrogels synthesized at nominal HA/peptide weight ratios: (a) 80/20, (b) 60/40, (c) 40/60 and (d) 20/80, scale bar = 200 nm. (e and f) Cryo-SEM images of hybrid hydrogels synthesized at a nominal 40/60 HA/peptide weight ratio. Insets show high magnification images with scale bar of 1 μm (e) and 250 nm (f). The arrows indicate the presence of apatite nanoparticles.

FTIR spectra of all samples showed phosphate vibrational bands ascribed to biomimetic apatite and the characteristic bands of Fmoc-FF (Fig. 4a). While the bands associated with the organic phase tend to disappear at increasing nominal HA/FF weight ratios, the phosphate vibrational bands became more prominent (Fig. 4a). In fact, the bar graph of the relative intensity of $\nu_3 PO_4$ at 565 cm^{-1} increased concomitantly with the increase of the initial HA/FF weight ratio, revealing that hybrid materials with a higher mineral content can be synthesized by varying the HA/FF ratio. Nonetheless, a higher mineral content resulted in heterogeneous hydrogels containing large aggregates of mineral outside the fibrils (extrafibrillar
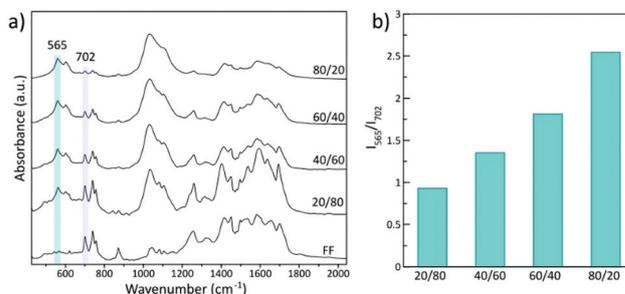

Fig. 4 (a) FTIR spectra of Fmoc-FF and hybrid xerogels synthesized at increasing nominal HA/FF weight ratios: 20/80, 40/60, 60/40 and 80/20. (b) Histogram of the ratio of IR peak intensity of Fmoc-FF with respect to HA (I_{565}/I_{702}).

This journal is © the Partner Organisations 2022

Inorg. Chem. Front., 2022, **9**, 743–752 | **747**

mineralization, Fig. 3). A compromise between the mineral content and organic matrix must be achieved to obtain hybrid hydrogels with uniform distribution of calcium phosphate nanoparticles. From these results we can infer the relevant role of the organic matrix in controlling apatite crystallization since a lower organic content that prompted random apatite crystallization ended up in micrometric aggregates. In this study, a nominal HA/FF weight ratio of 40/60 provides homogeneous integration of nanoparticles composed of calcium and phosphorus in the organic matrix (Fig. S4†). In addition, XRD patterns of hybrid materials display two broad bands at 26° and 32° (2θ) confirming the sole formation of poorly crystalline apatite (Fig. S5†).

To evaluate the impact that the corresponding HA/FF weight ratios have on the mechanical properties of the resulting hydrogels, samples with HA/FF weight ratios of 60/40, 40/60 and 20/80 were studied by shear rheology. In these samples, the ionic concentrations remained constant but the amount of the Fmoc-FF peptide varied significantly from 2.08 mM (ratio 60/40) to 4.68 mM (ratio 40/60) and 12.47 mM (ratio 20/80) (Table 2). First, note that all samples demonstrated a gel-like behaviour, characterized by the storage modulus (G') values larger by approximately an order of magnitude than the loss modulus (G'') values within the LVR, as well as trends of these moduli are approximately independent of the frequency of oscillation in frequency sweep tests (Fig. 5). Furthermore, the rheological results demonstrate that the gels became more robust (larger G' and G'' values) as the peptide concentration increased. This result is consistent with previous works of our group and other groups on peptide gels.[19,26] However, interestingly, the mean values of G' corresponding to the LVR (Fig. 5a) differ in magnitude from the values we recently reported in another work[26] for Fmoc-FF gels (not containing HA) for a similar amount of peptide (Table S1†): 4986 Pa for 12.47 mM Fmoc-FF in the present work (sample 20/80) vs. 4031 Pa for 10 mM Fmoc-FF in the previous work; 1146 Pa for 4.68 mM in the present work vs. 400 Pa for 5 mM in the previous work; approx. 291 Pa for 2.08 mM in the present work vs. 106 Pa for 2.5 mM in the previous work. The comparatively stronger nature of the gels of the present work at the two lowest Fmoc-FF concentrations with respect to the previous work, must be related to the non-negligible role of HA in the mechanical properties of the gels. However, at the highest Fmoc-FF concentration, this is not held-note that ratios of values of the current work against the previous work are 12.47/10 = 1.25 for peptide concentration and G' of 4985.828/4030.504 = 1.237. Therefore, it seems that at the highest concentration under study in the present work, the combined effects of HA and Fmoc-FF did not result in an increase of the value of G' with respect to the Fmoc-FF gel. The likely reason is the competition of the phosphate ion and Fmoc-FF for calcium ions in Fmoc-FF-HA samples, which would limit the assembly of peptides. To support this hypothesis, we characterized the mechanical properties of two more samples, based on the Fmoc-FF/HA sample at a ratio of 40/60, with the sole difference of not adding phosphate in one case, and doubling the content of
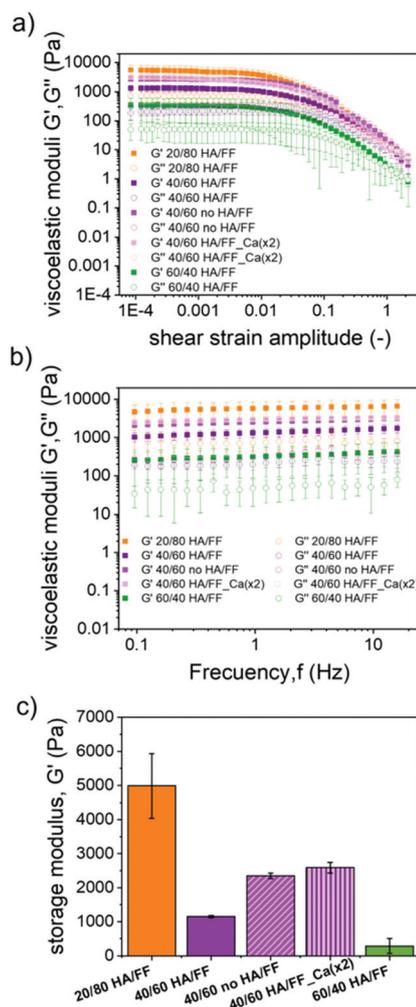

Fig. 5 Mechanical characterization of hybrid Fmoc-FF hydrogels in the different HA/peptide ratios (20/80, 40/60 and 60/40) under oscillatory shear. (a) Amplitude seeps: viscoelastic moduli as a function of shear strain amplitude for experiments under imposed oscillatory strains of 1 Hz fixed frequency. (b) Frequency sweeps: viscoelastic moduli as a function of shear strain frequency for experiments under imposed oscillatory strains of fixed amplitude, $\gamma_0 = 10^{-3}$. (c) Mean values and standard deviations of the values of the storage modulus corresponding to the linear viscoelastic region, as obtained from amplitude sweep experiments.

calcium ions in the other, both with respect to the reference sample. As observed, both modifications resulted in a more than two-fold increase in the value of G' with respect to the reference sample (Fig. 5c), supporting the hypothesis of the competition between peptides and the phosphate ions for the Ca^{2+} ion.

We also evaluated the influence of calcium concentration on peptide self-assembly and mineralization. Interestingly, TEM images of the sample having the lowest amount of Ca^{2+} (2 mM) showed the presence of the typical mesh of peptide fibers in which some of the fibers appeared fully mineralized (Fig. 6).

A deeper analysis of the fiber composition was carried out by STEM-EDS (Fig. 7). The HAADF-STEM image showed less
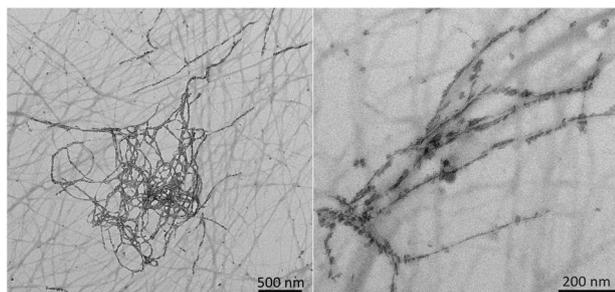
Fig. 6 TEM images of Fmoc-FF hydrogels mineralized with the lowest calcium concentrations (2 mM).
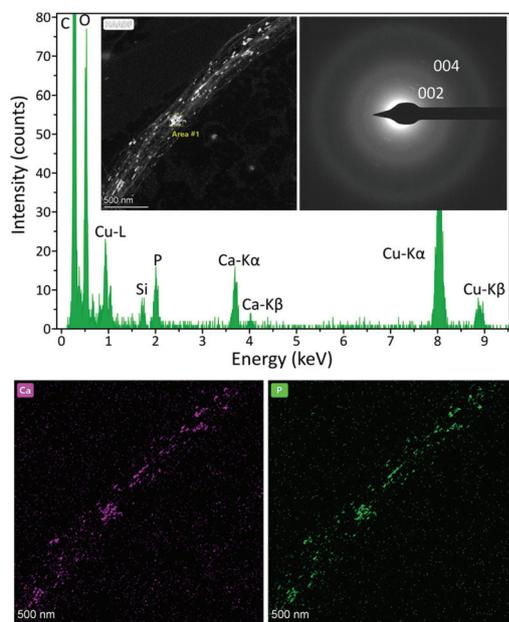

Fig. 7 HAADF-STEM micrograph, EDS spectrum and SAED patterns of a mineralized fibril. EDS maps showing the spatial distribution of Ca and P are also shown. The c-axis (002 and 004 reflections) of the nanocrystals are specifically oriented within the fibril.

bright peptide fibers and the presence of relatively heavy elements in the peptide fiber. The individual elemental maps reveal the relative position of Ca and P clearly demonstrating the formation of calcium phosphate nanoparticles within the fiber (Fig. 7). In addition, the SAED pattern of the same mineralized fiber displays arc-shaped 002 and 004 reflections indicating that the c-axis of apatite nanocrystals was aligned with the longitudinal axis of the peptide fiber (Fig. 7). This ordered arrangement of apatite nanocrystals within the fiber is similar to that found in biological mineralized collagen fibrils.[49] These observations suggest that mineralization occurs inside the fibers at a lower Ca^{2+} concentration, probably due to the specific interaction of all the available Ca^{2+} with the peptide fibers. As the concentration of Ca^{2+} increases in the media, HA nanocrystals can grow outside of the fibers, as observed in samples having a higher amount of Ca^{2+} ions (Fig. S6†).

To evaluate the impact that the increasing amounts of Ca^{2+} ions had on the mechanical properties of the hydrogels, samples having a Fmoc-FF concentration of 4.7 mM and increasing Ca^{2+} concentrations of 2 mM, 8.3 mM, 11.11 mM, 16.67 mM and 33.3 mM were measured by rheology (Fig. 8). As observed, the curves of amplitude sweeps and frequency sweeps demonstrated similar trends in all cases, typical of gel-like samples (see the previous discussion in Fig. 5), the only relevant effect of Ca^{2+} addition being the approximately linear enhancement of G' and G'' with the concentration of this ion (Fig. S7†).

As Ca^{2+} ions are responsible for the process of self-assembly and, therefore, hydrogel formation, the impact of this ion on the kinetics of gel formation was also evaluated macroscopically by rheology (Fig. S8†). Samples having different calcium concentrations demonstrated similar gelation kinetics, without any clear trend as the calcium concentration increased. In all cases, a fast gelation process was observed and the stationary values of $\tan \delta = G''/G'$ were achieved only after a few seconds. Note that at the stationary state $0.1 < \tan \delta < 1$, which is typical of weak gels.[61]
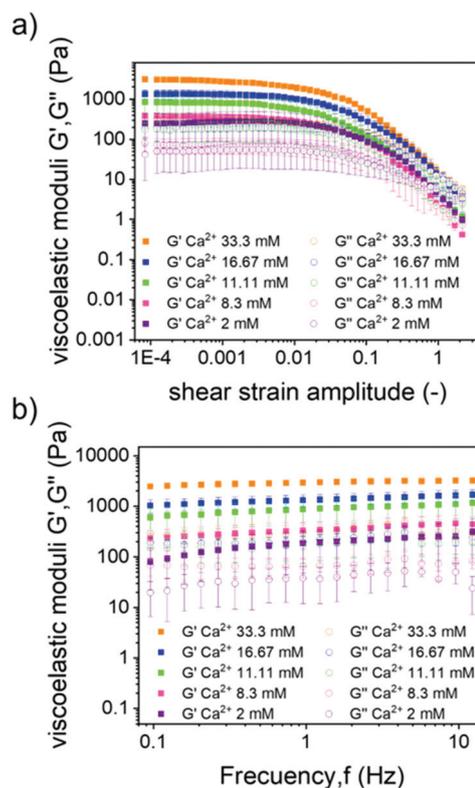
Fig. 8 Mechanical properties of hybrid hydrogels with different Ca^{2+} concentrations (2 mM, 8.3 mM, 11.11 mM, 16.67 mM and 33.3 mM). (a) viscoelastic moduli as a function of shear strain amplitude for experiments under imposed oscillatory strains of 1 Hz fixed frequency. (b) Viscoelastic moduli as a function of shear strain frequency for experiments under imposed oscillatory strains of fixed amplitude, $\gamma_0 = 10^{-3}$.

This journal is © the Partner Organisations 2022

Inorg. Chem. Front., 2022, **9**, 743–752 | **749**

Conclusions

We have developed a simple synthesis protocol in which the formation of the organic matrix and nanoapatite occurs simultaneously. We show that the amount of Ca^{2+} present in the media is essential for obtaining a fully composite material in which nanoapatite crystals are embedded, perfectly oriented, in the organic matrix, as occurring during collagen mineralization in bone. By studying the micro- and mechanical properties of the resulting hybrid hydrogels we have demonstrated that peptide self-assembly and mineral growth compete for Ca^{2+} ions present in the media. This effect has implications on the micro and macroscopic properties of the hybrid hydrogels and in the final fiber composition. Competition for Ca^{2+} ions in the organic matrix modulates crystal growth in a more precise way, emulating the natural process. This protocol demonstrates some of the properties that self-assembled systems can have in the development of complex materials and shed light on how nature uses them to exert a more precise control in biomineralization processes.

Author contributions

M. C. M.-T.: conceptualization, formal analysis, investigation, validation, visualization. G. B. R. R.: conceptualization, methodology, investigation, formal analysis, writing-original draft, writing – review & editing. J. I. G.-P.: conceptualization, formal analysis, investigation, validation. B. P. T.: conceptualization, formal analysis, investigation. J. M. C.: formal analysis, writing-original draft. M. T. L.-L.: methodology, formal analysis, writing-original draft. L. A. C.: conceptualization, funding acquisition, methodology, project administration, supervision, writing-original draft, writing – review & editing. J. M. D. L.: conceptualization, funding acquisition, methodology, project administration, supervision, writing-original draft, writing – review & editing.

Conflicts of interest

There are no conflicts to declare.

Acknowledgements

References

1 G. Wei, Z. Su, N. P. Reynolds, P. Arosio, I. W. Hamley, E. Gazit and R. Mezzenga, Self-assembling peptide and protein amyloids: From structure to tailored function in nanotechnology, *Chem. Soc. Rev.*, 2017, **46**, 4661–4708.

2 C. Yuan, W. Ji, R. Xing, J. Li, E. Gazit and X. Yan, Hierarchically oriented organization in supramolecular peptide crystals, *Nat. Rev. Chem.*, 2019, **3**, 567–588.

3 A. Levin, T. A. Hakala, L. Schnaider, G. J. L. Bernardes, E. Gazit and T. P. J. Knowles, Biomimetic peptide self-assembly for functional materials, *Nat. Rev. Chem.*, 2020, **4**, 615–634.

4 A. Lampel, Biology-Inspired Supramolecular Peptide Systems, *Chem*, 2020, **6**, 1222–1236.

5 K. Tao, A. Levin, L. Adler-Abramovich and E. Gazit, Fmoc-modified amino acids and short peptides: Simple bio-inspired building blocks for the fabrication of functional materials, *Chem. Soc. Rev.*, 2016, **45**, 3935–3953.

6 S. Fleming and R. V. Ulijn, Design of nanostructures based on aromatic peptide amphiphiles, *Chem. Soc. Rev.*, 2014, **43**, 8150–8177.

7 E. R. Draper and D. J. Adams, Low-Molecular-Weight Gels: The State of the Art, *Chem*, 2017, **3**, 390–410.

8 J. J. Panda, R. Dua, A. Mishra, B. Mittra and V. S. Chauhan, 3D cell growth and proliferation on a RGD functionalized nanofibrillar hydrogel based on a conformationally restricted residue containing dipeptide, *ACS Appl. Mater. Interfaces*, 2010, **2**, 2839–2848.

9 E. J. Berns, Z. Álvarez, J. E. Goldberger, J. Boekhoven, J. A. Kessler, H. G. Kuhn and S. I. Stupp, A tenascin-C mimetic peptide amphiphile nanofiber gel promotes neurite outgrowth and cell migration of neurosphere-derived cells, *Acta Biomater.*, 2016, **37**, 50–58.

10 J. Liu, Z. Sun, Y. Yuan, X. Tian, X. Liu, G. Duan, Y. Yang, L. Yuan, H. C. Lin and X. Li, Peptide Glycosylation Generates Supramolecular Assemblies from Glycopeptides as Biomimetic Scaffolds for Cell Adhesion and Proliferation, *ACS Appl. Mater. Interfaces*, 2016, **8**, 6917–6924.

11 A. Friggeri, B. L. Feringa and J. Van Esch, Entrapment and release of quinoline derivatives using a hydrogel of a low molecular weight gelator, *J. Controlled Release*, 2004, **97**, 241–248.

12 J. J. Panda, A. Mishra, A. Basu and V. S. Chauhan, Stimuli responsive self-assembled hydrogel of a low Molecular weight free dipeptide with potential for tunable drug delivery, *Biomacromolecules*, 2008, **9**, 2244–2250.

13 R. Huang, W. Qi, L. Feng, R. Su and Z. He, Self-assembling peptide-polysaccharide hybrid hydrogel as a potential carrier for drug delivery, *Soft Matter*, 2011, **7**, 6222–6230.

14 M. Conejero-Muriel, J. A. Gavira, E. Pineda-Molina, A. Belsom, M. Bradley, M. Moral, J. D. García-López Durán, A. Luque González, J. J. Díaz-Mochón, R. Contreras-Montoya, Á. Martínez-Peragón, J. M. Cuerva and L. Álvarez De Cienfuegos, Influence of the chirality of short peptide

750 | *Inorg. Chem. Front.*, 2022, **9**, 743–752

This journal is © the Partner Organisations 2022

supramolecular hydrogels in protein crystallogenesis, *Chem. Commun.*, 2015, **51**, 3862–3865.

15 R. Contreras-Montoya, G. Escolano, S. Roy, M. T. Lopez-Lopez, J. M. Delgado-López, J. M. Cuerva, J. J. Díaz-Mochón, N. Ashkenasy, J. A. Gavira and L. Álvarez de Cienfuegos, Catalytic and Electron Conducting Carbon Nanotube–Reinforced Lysozyme Crystals, *Adv. Funct. Mater.*, 2019, **29**, 1807351.

16 R. Contreras-Montoya, A. Castellví, G. Escolano-Casado, J. Juanhuix, M. Conejero-Muriel, M. T. Lopez-Lopez, J. M. Cuerva, L. Álvarez De Cienfuegos and J. A. Gavira, Enhanced Stability against Radiation Damage of Lysozyme Crystals Grown in Fmoc-CF Hydrogels, *Cryst. Growth Des.*, 2019, **19**, 4229–4233.

17 R. Contreras-Montoya, M. Arredondo-Amador, G. Escolano-Casado, M. C. Mañas-Torres, M. González, M. Conejero-Muriel, V. Bhatia, J. J. Díaz-Mochón, O. Martínez-Augustin, F. S. De Medina, M. T. Lopez-Lopez, F. Conejero-Lara, J. A. Gavira and L. álvarez De Cienfuegos, Insulin Crystals Grown in Short-Peptide Supramolecular Hydrogels Show Enhanced Thermal Stability and Slower Release Profile, *ACS Appl. Mater. Interfaces*, 2021, **13**, 11672–11682.

18 A. Dasgupta, J. H. Mondal and D. Das, Peptide hydrogels, *RSC Adv.*, 2013, **3**, 9117–9149.

19 L. Adler-Abramovich and E. Gazit, The physical properties of supramolecular peptide assemblies: From building block association to technological applications, *Chem. Soc. Rev.*, 2014, **43**, 6881–6893.

20 L. Chen, G. Pont, K. Morris, G. Lotze, A. Squires, L. C. Serpell and D. J. Adams, Salt-induced hydrogelation of functionalised-dipeptides at high pH, *Chem. Commun.*, 2011, **47**, 12071–12073.

21 L. Chen, T. O. McDonald and D. J. Adams, Salt-induced hydrogels from functionalised-dipeptides, *RSC Adv.*, 2013, **3**, 8714–8720.

22 A. Z. Cardoso, L. L. E. Mears, B. N. Cattoz, P. C. Griffiths, R. Schweins and D. J. Adams, Linking micellar structures to hydrogelation for salt-triggered dipeptide gelators, *Soft Matter*, 2016, **12**, 3612–3621.

23 K. McAulay, P. A. Ucha, H. Wang, A. M. Fuentes-Caparrós, L. Thomson, O. Maklad, N. Khunti, N. Cowieson, M. Wallace, H. Cui, R. J. Poole, A. Seddon and D. J. Adams, Controlling the properties of the micellar and gel phase by varying the counterion in functionalised-dipeptide systems, *Chem. Commun.*, 2020, **56**, 4094–4097.

24 S. Roy, N. Javid, P. W. J. M. Frederix, D. A. Lamprou, A. J. Urquhart, N. T. Hunt, P. J. Halling and R. V. Ulijn, Dramatic specific-ion effect in supramolecular hydrogels, *Chem. – Eur. J.*, 2012, **18**, 11723–11731.

25 W. Ji, C. Yuan, S. Zilberzwige-Tal, R. Xing, P. Chakraborty, K. Tao, S. Gilead, X. Yan and E. Gazit, Metal-Ion Modulated Structural Transformation of Amyloid-Like Dipeptide Supramolecular Self-Assembly, *ACS Nano*, 2019, **13**, 7300–7309.

26 M. C. Mañas-Torres, C. Gila-Vilchez, F. González-Vera, J. A. Conejero-Lara, V. Blanco, J. M. Cuerva, A. Lopez-Lopez,

M. T. Orte and L. Alvarez de Cienfuegos, In situ real-time monitoring the mechanism of self-assembly of short peptide supramolecular polymers, *Mater. Chem. Front.*, 2021, **5**, 5452–5462.

27 V. M. P. Vieira, L. L. Hay and D. K. Smith, Multi-component hybrid hydrogels-understanding the extent of orthogonal assembly and its impact on controlled release, *Chem. Sci.*, 2017, **8**, 6981–6990.

28 T. Shao, N. Falcone and H. B. Kraatz, Supramolecular Peptide Gels: Influencing Properties by Metal Ion Coordination and Their Wide-Ranging Applications, *ACS Omega*, 2020, **5**, 1312–1317.

29 L. Chen, S. Revel, K. Morris, D. G. Spiller, L. C. Serpell and D. J. Adams, Low molecular weight gelator-dextran composites, *Chem. Commun.*, 2010, **46**, 6738–6740.

30 G. Pont, L. Chen, D. G. Spiller and D. J. Adams, The effect of polymer additives on the rheological properties of dipeptide hydrogelators, *Soft Matter*, 2012, **8**, 7797–7802.

31 J. Nanda, B. Adhikari, S. Basak and A. Banerjee, Formation of hybrid hydrogels consisting of tripeptide and different silver nanoparticle-capped ligands: Modulation of the mechanical strength of gel phase materials, *J. Phys. Chem. B*, 2012, **116**, 12235–12244.

32 R. Contreras-Montoya, A. B. Bonhome-Espinosa, A. Orte, D. Miguel, J. M. Delgado-López, J. D. G. Duran, J. M. Cuerva, M. T. Lopez-Lopez and L. Á. de Cienfuegos, Iron nanoparticles-based supramolecular hydrogels to originate anisotropic hybrid materials with enhanced mechanical strength, *Mater. Chem. Front.*, 2018, **2**, 686–699.

33 B. Adhikari and A. Banerjee, Short peptide based hydrogels: Incorporation of graphene into the hydrogel, *Soft Matter*, 2011, **7**, 9259–9266.

34 S. Roy and A. Banerjee, Functionalized single walled carbon nanotube containing amino acid based hydrogel: A hybrid nanomaterial, *RSC Adv.*, 2012, **2**, 2105–2111.

35 D. Iglesias, M. Melle-Franco, M. Kurbasic, M. Melchionna, M. Abrami, M. Grassi, M. Prato and S. Marchesan, Oxidized Nanocarbons-Tripeptide Supramolecular Hydrogels: Shape Matters!, *ACS Nano*, 2018, **12**, 5530–5538.

36 N. Reznikov, J. A. M. Steele, P. Fratzl and M. M. Stevens, A materials science vision of extracellular matrix mineralization, *Nat. Rev. Mater.*, 2016, **1**, 1–14.

37 M. Llusar and C. Sanchez, Inorganic and hybrid nanofibrous materials templated with organogelators, *Chem. Mater.*, 2008, **20**, 782–820.

38 D. J. Adams, L. M. Mullen, M. Berta, L. Chen and W. J. Frith, Relationship between molecular structure, gelation behaviour and gel properties of Fmoc-dipeptides, *Soft Matter*, 2010, **6**, 1971–1980.

39 C. Gila-Vilchez, M. C. Mañas-Torres, J. A. Gonzalez Vera, F. Franco-Montalban, J. A. Tamayo, F. Conejero-Lara, J. M. Cuerva, M. T. Lopez-Lopez, A. Orte and L. Alvarez de Cienfuegos, Insights into the co-assemblies formed by different aromatic short-peptides amphiphiles, *Polym. Chem.*, 2021, **12**, 6832.

This journal is © the Partner Organisations 2022

Inorg. Chem. Front., 2022, **9**, 743–752 | **751**

40 S. Cavalli, F. Albericio and A. Kros, Amphiphilic peptides and their cross-disciplinary role as building blocks for nanoscience, *Chem. Soc. Rev.*, 2010, **39**, 241–263.

41 J. D. Hartgerink, E. Beniash and S. I. Stupp, Self-assembly and mineralization of peptide-amphiphile nanofibers, *Science*, 2001, **294**, 1684–1688.

42 Z. A. C. Schnepp, R. Gonzalez-McQuire and S. Mann, Hybrid biocomposites based on calcium phosphate mineralization of self-assembled supramolecular hydrogels, *Adv. Mater.*, 2006, **18**, 1869–1872.

43 M. Ghosh, M. Halperin-Sternfeld, I. Grigoriants, J. Lee, K. T. Nam and L. Adler-Abramovich, Arginine-presenting peptide hydrogels decorated with hydroxyapatite as biomimetic scaffolds for bone regeneration, *Biomacromolecules*, 2017, **18**, 3541–3550.

44 C. J. Newcomb, R. Bitton, Y. S. Velichko, M. L. Snead and S. I. Stupp, The role of nanoscale architecture in supramolecular templating of biomimetic hydroxyapatite mineralization, *Small*, 2012, **8**, 2195–2202.

45 R. Zhang and P. X. Ma, Biomimetic polymer/apatite composite scaffolds for mineralized tissue engineering, *Macromol. Biosci.*, 2004, **4**, 100–111.

46 G. Wei and P. X. Ma, Structure and properties of nano-hydroxyapatite/polymer composite scaffolds for bone tissue engineering, *Biomaterials*, 2004, **25**, 4749–4757.

47 F. Nudelman and N. A. J. M. Sommerdijk, Biomineralization as an Inspiration for Materials Chemistry, *Angew. Chem., Int. Ed.*, 2012, **51**, 6582–6596.

48 U. G. K. Wegst, H. Bai, E. Saiz, A. P. Tomsia and R. O. Ritchie, Bioinspired structural materials, *Nat. Mater.*, 2014, **14**, 23.

49 A. L. Boskey, Biomineralization: conflicts, challenges, and opportunities, *J. Cell. Biochem. Suppl.*, 1998, **30–31**, 83–91.

50 G. B. Ramírez-Rodríguez, T. M. F. Patrício and J. M. Delgado-López, Natural polymers for bone repair, in *Bone Repair Biomaterials*, Woodhead Publishing, 2019, pp. 199–232.

51 Y. Wang, T. Azaïs, M. Robin, A. Vallée, C. Catania, P. Legriel, G. Pehau-Arnaudet, F. Babonneau, M.-M. Giraud-Guille and N. Nassif, The predominant role of collagen in the nucleation, growth, structure and orientation of bone apatite, *Nat. Mater.*, 2012, **11**, 724–733.

52 J. M. Delgado-López, M. Iafisco, I. Rodríguez, A. Tampieri, M. Prat and J. Gómez-Morales, Crystallization of bioinspired citrate-functionalized nanoapatite with tailored carbonate content, *Acta Biomater.*, 2012, **8**, 3491–3499.

53 J. M. Delgado-López, R. Frison, A. Cervellino, J. Gómez-Morales, A. Guagliardi and N. Masciocchi, Crystal Size, Morphology, and Growth Mechanism in Bio-Inspired Apatite Nanocrystals, *Adv. Funct. Mater.*, 2014, **24**, 1090–1099.

54 H. A. Lowenstam and S. Weiner, *On Biomineralization*, University Press, Oxford, 1989.

55 Y. Y. Hu, A. Rawal and K. Schmidt-Rohr, Strongly bound citrate stabilizes the apatite nanocrystals in bone, *Proc. Natl. Acad. Sci. U. S. A.*, 2010, **107**, 22425–22429.

56 J. Gómez-Morales, M. Iafisco, J. M. Delgado-López, S. Sarda and C. Drouet, *Progress in Crystal Growth and Characterization of Materials*, 2013, vol. 59, pp. 1–46.

57 H. Lu, A. Khan and P. G. Smirniotis, Relationship between structural properties and CO_2 capture performance of CaO− based sorbents obtained from different organometallic precursors, *Ind. Eng. Chem. Res.*, 2008, **47**, 6216–6220.

58 C. Gao, S. Peng, P. Feng and C. Shuai, Bone biomaterials and interactions with stem cells, *Bone Res.*, 2017, **5**, 1–33.

59 G. B. Ramírez-Rodríguez, J. M. Delgado-López, M. Iafisco, M. Montesi, M. Sandri, S. Sprio and A. Tampieri, Biomimetic mineralization of recombinant collagen type I derived protein to obtain hybrid matrices for bone regeneration, *J. Struct. Biol.*, 2016, **196**, 138–146.

60 G. B. Ramírez-Rodríguez, A. R. Pereira, M. Hermann, J. Hansmann, J. M. Delgado-López, S. Sprio, A. Tampieri and M. Sandri, Biomimetic mineralization promotes viability and differentiation of human mesenchymal stem cells in a perfusion bioreactor, *Int. J. Mol. Sci.*, 2021, **22**, 1–15.

61 A. Borzacchiello, F. Della Sala and L. A. Ambrosio, *Rheometry of polymeric biomaterials*, Woodhead Publishing, 2017, pp. 233–253.

752 | *Inorg. Chem. Front.*, 2022, **9**, 743–752

This journal is © the Partner Organisations 2022